Precision Measurements of the Autoionizing States of Strontium in an Electric Field

A thesis submitted in partial fulfillment of the requirement
for the degree of Bachelor of Science with Honors in
Physics from the College of William and Mary in Virginia,

by

Kathy-Anne Brickman

Accepted for _____

(Honors, High Honors, or Highest Honors)

_____

Advisor: Dr. William E. Cooke

_____

Director: Dr. Keith Griffioen

_____

Dr. John Delos

_____

Dan Smith

Williamsburg, Virginia

April 2001

Table of Contents:

I.Abstract ____ 3

II. Introduction ____ 3

A. Field Background ____ 8

III. Theory ____ 9

A. Zero Field ____ 9

B. Electric Field ____ 14

C. Frequencies ____ 16

IV. Experiment ____ 18

A. Lasers ____ 18

B. Apparatus ____ 23

C. Calibration ____ 24

IV. Data Analysis ____ 27

A. Electric Field ____ 32

B. Laser Resolution ____ 34

V. Conclusions ____ 36

VI. Future Work ____ 37

VII. Acknowledgements ____ 37

VIII. References: ____ 37

Precision Measurements of the Auto-ionizing States of Strontium in an Electric Field

Kathy-Anne Brickman

I.Abstract

This paper presents a technique for making precision measurements of auto-ionizing states of strontium in an electric field. The spectrum of the $4d_{3/2}nl$ and the $4d_{5/2}n'l'$ states in a Stark field exhibit interference between the Stark field interaction, and interactions between the quadrupole moment of the core and the Rydberg electron. The Stark field also narrows the auto-ionizing resonances so that a precision measurement can identify the presence of periodic orbits in this complex system.

II. Introduction

In a classical view atoms consist of an electron cloud orbiting a nucleus. The electron cloud contains levels that the orbiting electrons can fill. The level an electron occupies is determined by the angular momentum, l, of the electron. The core contains a charged nucleus and filled electron shells. Strontium has two valence electrons in its outer shell. Through laser excitation it is possible to excite one of the electrons to higher states where it becomes a Rydberg electron. Rydberg electrons are just electrons which lie a few levels above the valence shell. Strontium has a precessing quadrupole moment core in its 4dnl levels. A quadrupole moment is a non-isotropic charge distribution that has a dumbbell shape. This dumbbell shape charge distribution precesses about the core electron's spin and orbital angular momentum.

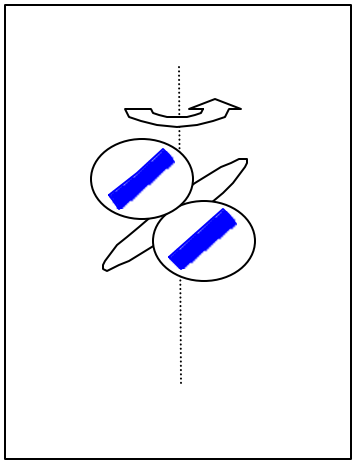

Figure 1: Precession of a quadrupole core. The angular momentum, L, and spin, S, precess about J.

Classically, the Rydberg electron orbits around the core in an elliptical pattern. The electron is in an nl state.

As it travels around the core it causes the core to flip from one fine structure state to the other, while the orbiting electron makes a transition from one nl value to a different n'l'. This is illustrated in Fig.2. If an atom is originally in the $4d_{3/2}15l$ state, when the Rydberg electron passes the core it causes the core to switch from $4d_{3/2}$ state to a $4d_{5/2}$ state. This is due to the coupling of the orbital

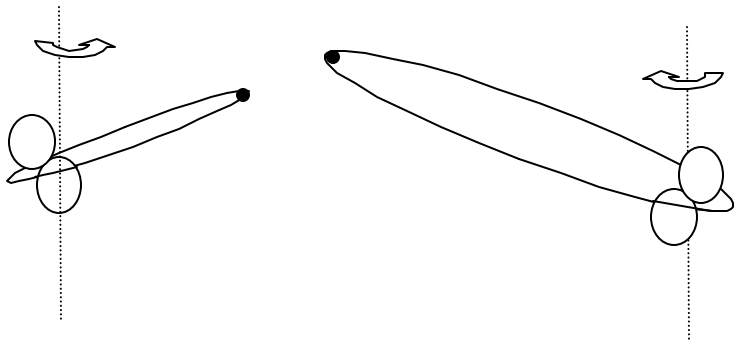

Figure 2:Electron-core interaction. The configuration of the atom prior to the outer electron orbiting the core (right), the atom is in a $4d_{3/2}15f$ configuration. After it passes the core, the electron is in the $4d_{5/2}11f$ configuration (left).

angular momentum of the two electrons. In response the orbiting electron transitions from a 15l state into an 11l' state. The resulting atom is in the $4d_{5/2}11l$ state. If in addition an electric field is applied, it provides a torque perpendicular to the field axis. Therefore only $L_{z,}$ which corresponds to m, is a good quantum number. States with different l values are coupled to each other, but all

the states coupled have the same m value. This results in a precession of the entire orbit, the greater the field strength the greater the precession rate.

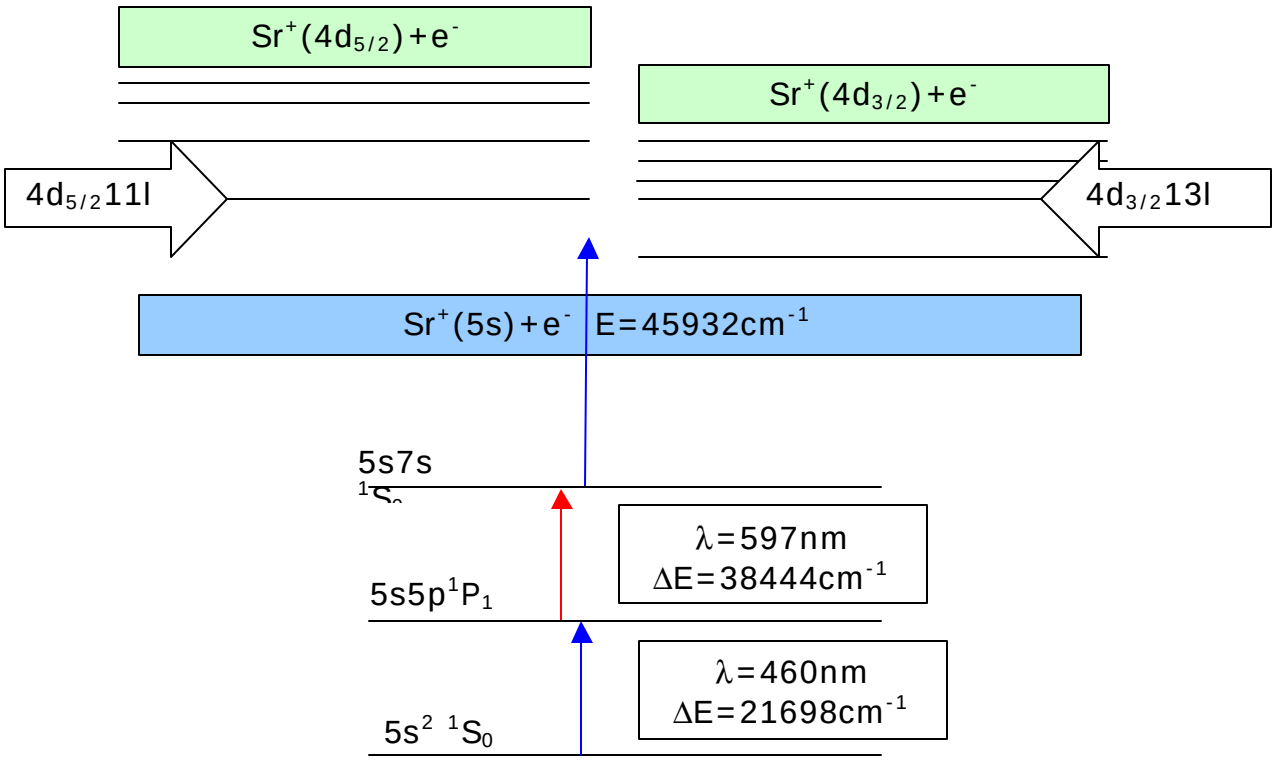

Figure 3: Energy Level Diagram for strontium. Three-photon excitation excited strontium to 4dnl levels, with each transition parity and angular momentum changed.

We used three-photon step-wise excitation to excite strontium from its ground state to the 4dnl Rydberg levels above the $Sr^+(5s)$ ionization limit. The diagram in Fig. 3 shows the intermediate states and energies needed to reach the 4dnl levels. We began in the $5s^2\ ^1S_0$ ground state and our first transition was to the $5s5p\ ^1P_1$ state. A transition to this state is possible because The absorbed photon is odd parity and carries one unit of angular momentum therefore a transition to the $5s5p\ ^1P_1$ state is possible because the parity of the state changes and l changes. The next excitation was to the $5s7s\ ^1S_0$, for which the parity and angular momentum had to also change accordingly. In order to reach the odd-parity J=1 4dnl levels our last intermediate state had to be a J=0 even-parity state, the $5s7s^1S_0$. The $5s7s^1S_0$ state is mixed with the $5p^2\ ^1S_0$ and $4d^2\ ^1S_0$ states. This mixing allows the transition to the

4dnl states. It is much easier to go from a $4d^2$ state to a 4dnl state because it does not involve a core transition as going from a $5s^2$ to a 4dnl state would. The transition is therefore easier because it is a one-electron transition and not a two-electron transition. The $4d_{5/2}11l$ and the $4d_{3/2}13l$ states have the largest effect from the interaction between the Rydberg and core electron because they are nearly degenerate, as the picture below illustrates. Moreover, the $4d_{5/2}12l$ is also degenerate with the $4d_{3/2}15l$ state. This maximizes the perturbations.

We are looking at odd parity J=1 states. Most past work for strontium is for even parity J=0,J=2 and odd parity J=3 states. Other than vacuum ultra-violet (VUV) spectra not much data is available for the low-lying J=1 odd parity states. Hudson, Carter, and Young[1] first examined the J=1 odd states of strontium. They looked at the absorption spectrum in the region of 1646-2028 Angstroms. Vacuum UltraViolet excitation was used to reach the 4dnl levels. The main focus of Hudson's paper was to identify states in the 4d region. Peter Esherick studied the bound, even parity J=0 and $J=2^2$ spectra of strontium. Esherick used MQDT, multi-channel quantum defect theory, to predict experimental results and then matched predictions to his own experiment to see how they correlated. This spectrum is very well understood and his experimental data fit his MQDT model. Aymar, Luc-Koenig, and Wantanbe[3] produced R-matrix calculations of eigenchannel multichannel quantum defect parameters for strontium. Each channel is a Rydberg series of strontium; multi-channel calculations typically include many series. They showed that channel mixing was prevalent in strontium and that as the calculation included more channels the more accurate the results became. Aymar went on to study the problem in more detail. In 1987 her paper[4] on eigenchannel R-matrix calculations of the photoabsorption spectrum of strontium predicted the positions and shapes of the $4d_{3/2,5/2}np$ and the $5p_{1/2,3/2}n$'s states. She showed that through the use of many channels with an MQDT calculation the positions and shapes of the peaks of the 4d and 5p states could be achieved.

Her MQDT analysis was heavily energy-dependent and exact calculations about peak positions could not be made. Aymar (et al.) continued work on strontium by looking at the J=3 auto-ionizing spectrum of strontium up to the 4d ionization threshold[5]. Similar perturbations among states were found in the strongly perturbed regions where the two 4d series overlap in the J=3 spectrum also. Next Aymar and Camus[6] looked at the even-parity J=0 auto-ionizing spectrum of strontium below the $4d_{5/2}$ threshold. High lying states were predicted and observed. Most attention has been given to states with high n's and very little has been done for the region between the $4d_{5/2}$nl and $4d_{3/2}$ nl regions where the two series overlap. The previous experiments and theoretical analysis conclude that the area in the overlapping region of the $4d_{3/2}$nl levels and $4d_{5/2}$n'l' is strongly perturbed.

Various groups have studied other alkaline earth elements to see if strong state mixing existed in the spectra as well. Greene and Aymar[7] looked at spin orbit effects in the heavy alkaline earth elements. Strontium was among the elements studied, but only for high n values. They compare the techniques of MQDT and R-matrix calculations with experimental data. Nuekammer and Rinneberg[8] studied the configuration interaction and singlet-triplet mixing probed by hyperfine structure of barium Rydberg states. Discrepancies were found between their experiment and MQDT theory.

MQDT normally describes the interactions in the area of degeneracies, but since strontium requires a heavily energy dependent MQDT analysis, in the overlapping regions MQDT is not a very good description of what is happening. Strontium's dramatic structure in this area leads us to believe that more than coupling between states produces rapid changes in the spectra. We believe that since the 4dnl levels lie close to strontium's core it is the interaction with the core that leads to the complications. Possibly the 4d shell is on the verge of collapsing into to the core. Rubidium lies to the left of strontium and Yttrium lies to the right. In Rubidium the 4d

orbital lies above the 5s and 5p orbitals. In neutral strontium the 4d orbital has dropped below the 5s orbital and lies between the 5s and 5p orbitals, being closer to the 5p orbital. In Sr^+, the series we are studying, the 4d orbital has dropped even closer to the 5s orbital. By the time Yttrium is reached the 4d orbital has dropped below the 5p and 5s orbitals. We believe that in Sr^+ the 4d orbital is on the verge of collapsing into the core and any small change in the core will pull it further into the core.

A. Field Background

All past work for atoms in an electric field is for one electron systems and two electron systems with an isotropic core. Harmin did a great deal of work with atoms in an electric field. Most of his work has used QDT, quantum defect theory, to predict the effect of electric fields on atomic spectra. Harmin[9] studied the hydrogenic Stark effect in properties of the wave functions using a modified WKB treatment of a hydrogenic atom in a static electric field. He found his predictions accurate over all energies to within 1% for fields less than 5000kV/cm.

K. Sakimoto[10] extended Harmin's work to molecular hydrogen. This was the first experimental work done with non-isotropic cores. He studies the effect of Stark fields on H_2. He concludes that the spectra for the molecular case is much more difficult than for that of atoms due to the additional predissociaton channel which can compete with the auto-ionization channel. He says further studies between the effects of the two channels in hydrogen would be useful to explain the dynamics of the molecule. He suggests tuning the field strength to adjust the degree of importance of auto-ionization and predissociation. Sakimoto went on to study MQDT theory of the Stark effect.[11] He extended Harmin's work on alkali metals with a closed shell core to a general case in which the ion core is in an arbitrary state. His theory correlated well with numerical examples. In a later paper H.H. Fielding and T.P.

Softley[12] continued the studies of MQDT analysis of the Stark effect in auto-ionizing Rydberg states of H_2. They compare their calculations to their own previous experimental data. The data[13] showed that the field spectra changes a great deal from zero field spectra, but state identifications were nearly impossible.

Electric field effects on barium have also been studied. J.Neukammer and H. Rinneberg[14] study the effects of external fields on high-n Rydberg atoms with an isotropic 6s core. They looked at barium in Rydberg states at around n=290 as well as states of n between 70 and 160 in external electric and magnetic fields. Interference effects from the presence of non-hydrogenic states with the manifolds were observed and compared to calculations based on Harmin's work. Good correlation was found between theory and experiment for barium in an electric field. Robicheaux, Wesdorp, and Noordam looked at the Stark states and electron correlation in barium[15]. They formulated a theory to describe the Rydberg states of atoms and molecules in static electric fields.

Previous work shows that systems with isotropic cores are well-understood and that MQDT parameterizes the states efficiently. The work with molecular hydrogen shows that non-isotropic cores are difficult to work with. In the case of molecules predissociation is a major problem. Our experiment examines atomic strontium, and so predissociation does not play a role. Strontium has a non-isotropic core in its 4dnl states. This is the first experimental work done for a non-isotropic core in an atom.

III. Theory

A. Zero Field

For strontium the energy separations between Rydberg states scale with their quantum number as $1/(n^*)^3$. Here n^* is the effective principle quantum number. For high n states, n^{*3} becomes large and $1/n^{*3}$ becomes small. The interaction between

the inner quadrupole moment of the core electron and the outer Rydberg electron mixes configurations and produces energy shifts that complicate the spectrum.

At the 4d limit there are two states that the core electron can occupy, the $4d_{3/2}$ and the $4d_{5/2}$ fine structure states. These two states result from the coupling of the core electron's spin to that of the orbital angular momentum, l, of the core. The spin of the electron and orbital angular momentum are parallel for the $4d_{5/2}$ fine structure and anti-parallel for the $4d_{3/2}$ fine structure state. If the core is in a 4d configuration, then the Rydberg electron can be in either an np or an n'f configuration. The rules governing this scenario state that for each transition orbital angular momentum must change by 0 or 1 in either direction and parity must change. The atom begins in a 5s7s $^1S_0$ state which is mixed with the $4d^2$ $^1S_0$ state, both are even parity J=0 states so the only transitions possible are to the 4dnp $^1P_1$, 4dnp $^3P_1$, 4dnp $^3D_1$ and 4dnf $^1P_1$, 4dnf $^3P_1$, 4dnf $^3D_1$ odd parity, J=1 states. The area of interest for this project is in the region where the $4d_{3/2}$nl and $4d_{5/2}$n'l' states overlap.

For low n values the core electron and outer orbiting electron interact through LS coupling, that is the orbital angular momentum, L, and spin, S, couple together to produce J. The orbital angular momentum is equal to the sum of angular momentum from each electron, l. The components add through vector addition, meaning that L can range from the difference of the l's to the sum of the l's:

$$\vec{L} = \vec{l}_1 + \vec{l}_2 \qquad \textbf{(1)}$$

For example in the 4dnp state the core (4d) has orbital angular momentum $l_1=2$ and the outer electron (np) has orbital angular momentum $l_2=1$, so L=1,2,3. Similarly the spins,S, add in the same way:

$$\vec{S} = \vec{s}_1 + \vec{s}_2 \qquad \textbf{(2)}$$

For our two electrons $s_1=s_2=1/2$, so S=0 or 1.

The total angular momentum, J, of the system is equal to the vector sum of S and L.

$$\vec{J} = \vec{L} + \vec{S} \qquad \textbf{(3)}$$

In this example J=4,3,2,1,0.

In the 4dnp configuration 12 states are possible as shown in Fig. 4:

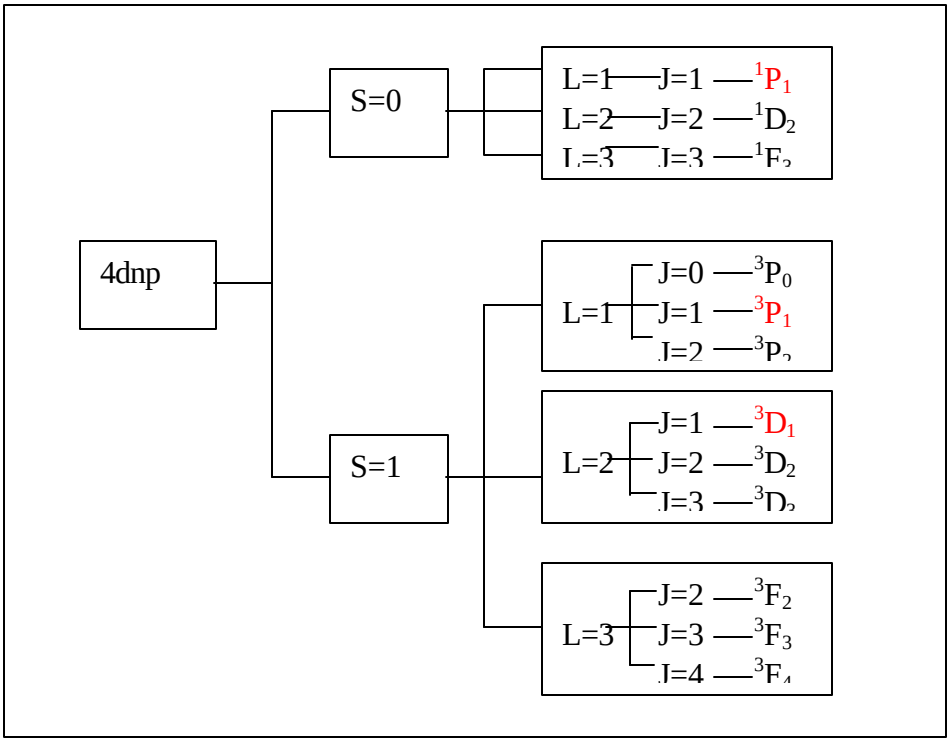

Figure 4: States available at the 4dnp level from a 5s7s $^1S_0$ state determined through L-S coupling. Our experiment examines odd parity J=1 states so only 3 of the 12 possible states are available to us.

The states are labeled using Russell-Saunders notation: $^{2S+1}L_J$. So the S=1, L=2, J=1 would be denoted $^3D_1$. The orbitals are labeled according to their L values, they are L=S,P,D,F for L=0,1,2,3 respectively. Thus D represents the L=2 orbital. The last intermediate stage was the 5s7s $^1S_0$ and since this experiment was for odd-parity J=1 states, only 3 of the 12 possible states were accessible to us; the 4dnp $^3P_1$, $^1P_1$,$^3D_1$, similarly in the 4dn'f configuration 3 states are accessible; 4dn'f $^3P_1$, $^1P_1$,$^3D_1$.

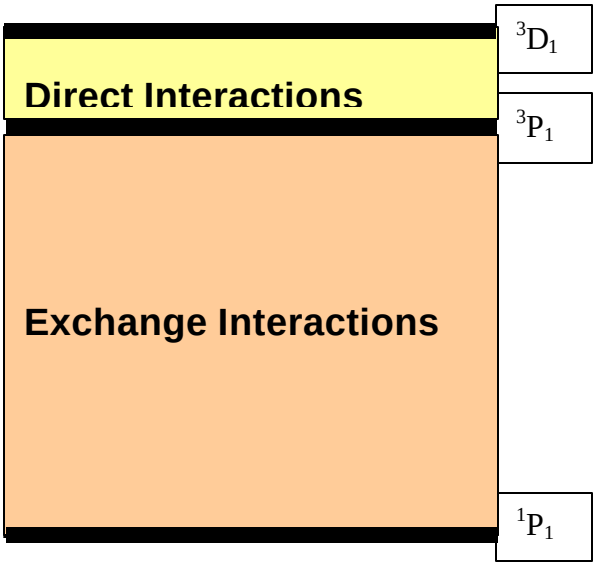

Figure 5 Interactions affecting singlet and triplet states.

The $^1P_1$ is a singlet state and the $^3P_1$, $^3D_1$ are triplet states. The difference in their energy spacings are determined by electrostatic interactions. The $^1P_1$ and $^3P_1$ states are split by the dipole and octopole exchange interactions. The $^3P_1$ and $^3D_1$ are split by the direct quadrupole interaction. All of these interactions arise from an expression of the electrostatic interaction, $1/r_{12}$, where r_{12} corresponds to the distance from the core electron to the Rydberg electron. As the outer electron gets close to the core, the interaction becomes stronger; as the electron gets further from the core, the interaction weakens. The distance of closest approach between the outer electron and the core electron effectively determines the interaction strength. Normalization of the wavefunction means that the density of Rydberg electrons inside the core decreases as $1/n^{*3}$ and so do the aforementioned interactions.

At high n values $1/r_{12}$ is greatly reduced and the electrostatic interactions become weak. In this region the configurations are determined by j-j coupling. The states still have odd parity and J=1, but the j-j description is better because the $4d_{3/2}$- $4d_{5/2}$ splitting is large compared to the electrostatic interaction. This coupling depends upon the total angular momentum of each electron, j_1 and j_2, which are added through vector addition as before. Therefore the only states accessible at high n values are: $4d_{3/2}np_{1/2}$, $4d_{3/2}np_{3/2}$, $4d_{3/2}nf_{5/2}$, $4d_{5/2}n'p_{3/2}$, $4d_{5/2}n'f_{5/2}$, $4d_{5/2}n'f_{7/2}$. The

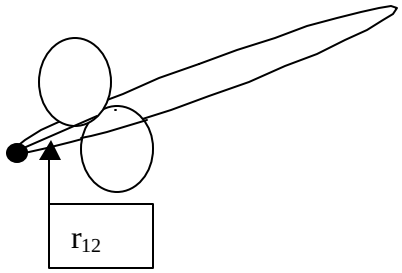

Figure 6: r_{12} is the distance of closest approach between the core and orbiting electron.

first three of these converge to the $4d_{3/2}$ fine structure limit and the other three converge to the $4d_{5/2}$ fine structure limit. In the areas of overlap between the two fine structure limits degeneracies occur. For example the $4d_{3/2}15p$ states are nearly degenerate with the $4d_{5/2}12p$ states. In these areas the electrostatic interactions dominate because the energy levels are so close to one another that the fine structure interaction is small compared to the electrostatic interaction. These electrostatic interactions complicate the spectrum by mixing states and making the two series indistinguishable from each other.

Configuration mixing occurs when the spacing between two states is so small that the normally small Coulomb interaction is larger than the unperturbed spacing. The states push apart through Coulomb interactions and neither state is then in its original configuration, but instead is in a linear superposition of the two interacting states. Beyond the $Sr^+(5s)$ ionization limit this configuration mixing also couples the 4dnl states with the 5s p states in the continuum. For doubly excited states neither electron alone has enough energy to escape the atom, but because the two states are configuration mixed they are able to exchange energy. Through an exchange interaction the electrons can transfer energy so that one electron has enough energy to escape. When the electron escapes the remaining part of the atom is an ion. Hence the atom auto-ionizes.

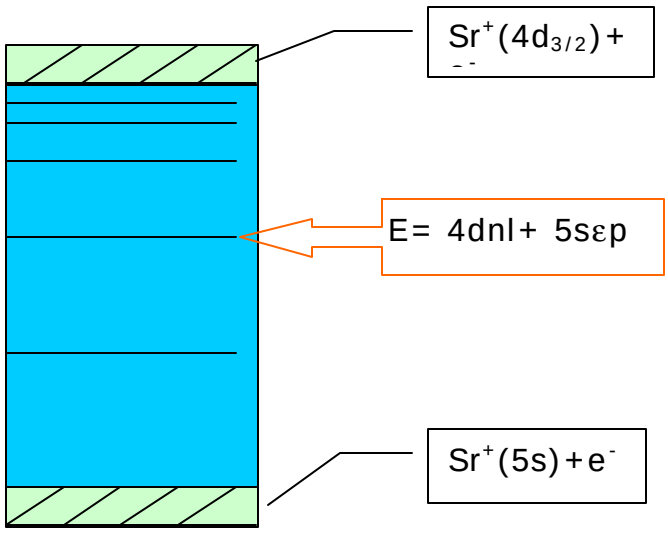

Figure 7: Due to configuration mixing a state in the 4dnl levels is also mixed with background from the Sr+(5s) continuum.

B. Electric Field

The presence of an electric field couples the high angular momentum states to the lower states. These high l states have no density inside the 4d core. Therefore the interaction between the 4dnl levels and the core is reduced because the distance between the core and outer electron is increased. The hydrogenic Stark model tells how the energy levels of hydrogen split in the presence of an electric field. The equation for the model is:

$$E=109737cm^{-1}/n^{*}(3/2)kn^{*}F2*(109737)/(5.25*10^{9})) \quad \textbf{(4)}$$

Here k is an integer ranging from (1-n) to (n-1), n* is the effective principle

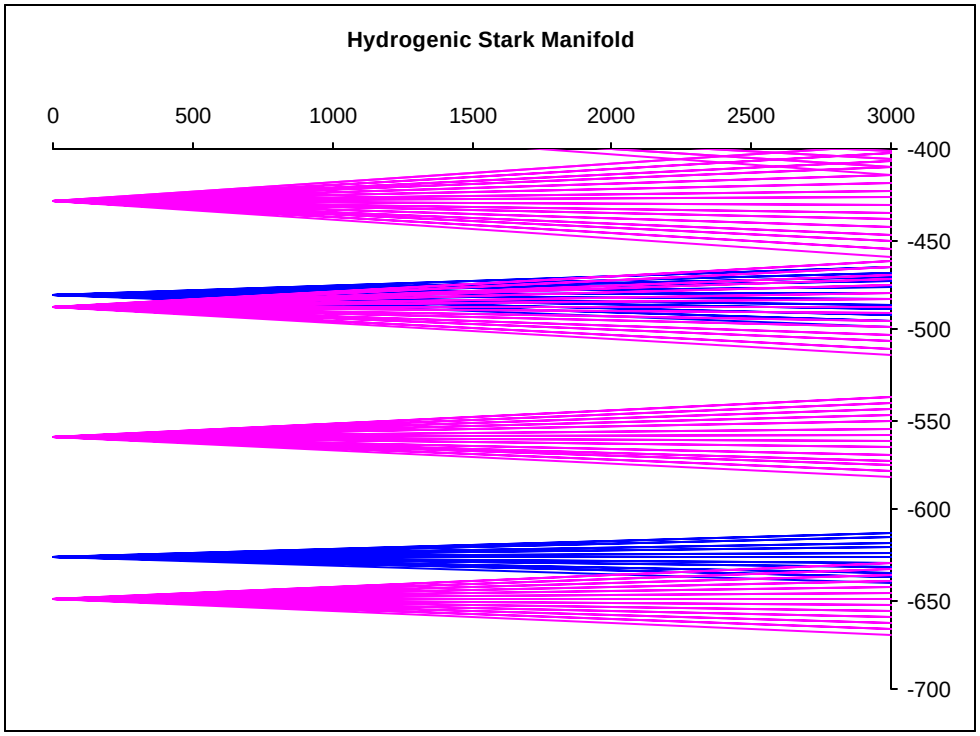

Figure 8: Stark manifold for strontium for $n_{3/2}$=16,15,14,13(in pink with n=16 at the top) and $n_{5/2}$=12,11(in blue with n=12 first). A great deal of crossings exist in this area.

quantum number, and F is field strength. Strontium differs from this model because there are small shifts that arise from strontium being a two-electron system. States

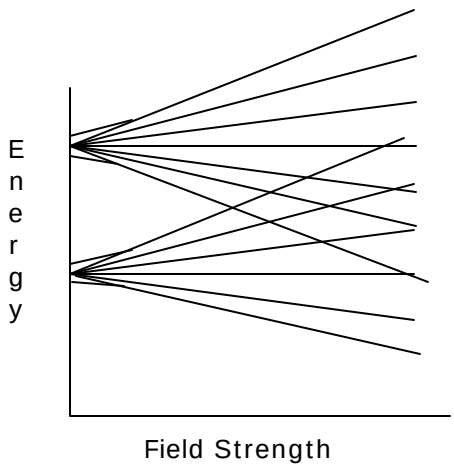

Figure 9 : Strontium differs from the hydrogenic model in that there are shifts on the edges of the manifolds that rejoin the model later.

at the edges are slightly shifted but rejoin the manifold later as shown. The model is still a good approximation. Anti-crossings occur where the manifolds overlap. Anti-crossings are regions where two energy lines would overlap but Coulomb forces push apart. The distance between the anti-crossings is a measure of interaction strength.

The Stark effect occurs when an electric field is applied to an atom. Stark splitting refers to how the energy levels split in an electric field. As can be seen in Fig. 8, the levels split in a comb-like fashion with

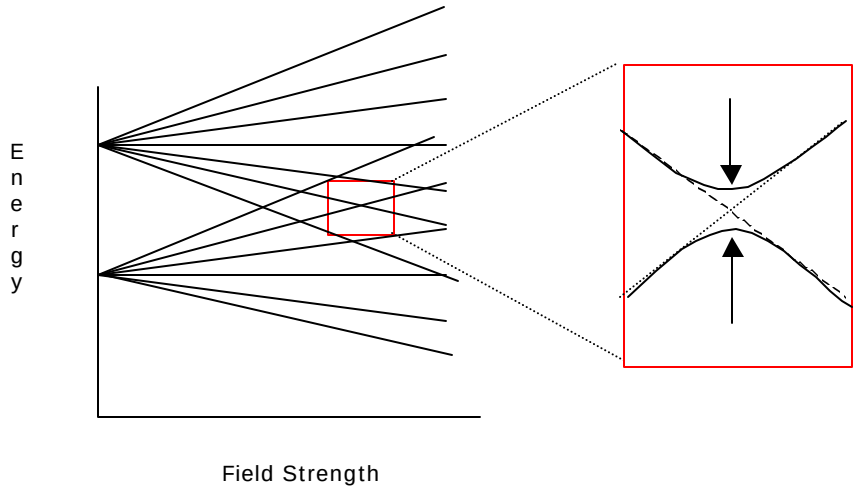

Figure10: In the region where spectral lines overlap anti-crossings occur. Instead of the lines crossing, coloumb interactions push them apart. The distance between the anti-crossings is a measure of interaction strength.

n splittings per energy level for the m=0 case. Here n is the principle quantum number and m is the magnetic quantum number. The picture also shows that the most

overlap occurs for the $4d_{5/2}12k$ and $4d_{3/2}15k'$ states. Although the $4d_{5/2}11k$ and $4d_{3/2}13k'$ are also nearly degenerate.

The areas of overlap in the Stark manifold are not trivially explained. One way of calculating what is happening in these areas is through quantal calculations. This procedure uses a large number of states, Stark energies, and multipole couplings. Calculations are possible but cumbersome and not insightful for a physical description of what is happening. Another method that is able to provide some physical insight is the semi-classical approach of Delos, which identifies periodic orbits that lead to scaling along a path of splittings. This theory is currently being developed.

C. Frequencies

Classically the interactions between the outer electron and the core can be explained through three frequencies. The spin orbit frequency, the Rydberg

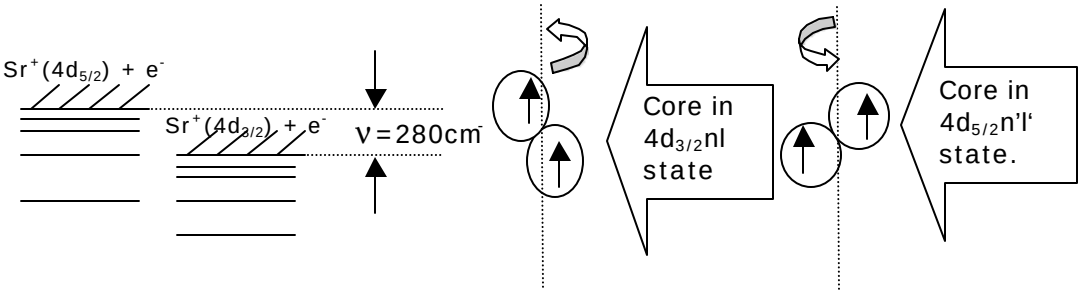

Figure 11: The spin orbit frequency is equal to the difference between the 4d ionization limits (above); physically it is how fast the core flips from one fine structure state to the other (below) Notice the direction of precession changes when the core flips states. The arrows inside the quadrupoles tell the direction of the spin.

frequency, and the Stark frequency, which are shown below. The spin orbit frequency is equal to the difference between the $4d_{3/2}$ and $4d_{5/2}$ ionization limits, $280cm^{-1}$. It corresponds to the rate the core switches from the $4d_{3/2}$ configuration to

the $4d_{5/2}$ configuration. As electrons approach the 4d limit, their series converge to one of the two ionization limits. The spacing between these converging series is equal to the Rydberg frequency of $1/(n^*)^3$. This is the frequency at which the outer electron orbits the core. The third frequency is the frequency associated with the electric field, the Stark frequency. The Stark frequency is equal to the spacing between two lines in the Stark manifold. It tells how fast the orbit precesses in an electric field. Our system has nearly degenerate energy levels for the $4d_{3/2}nl$ and

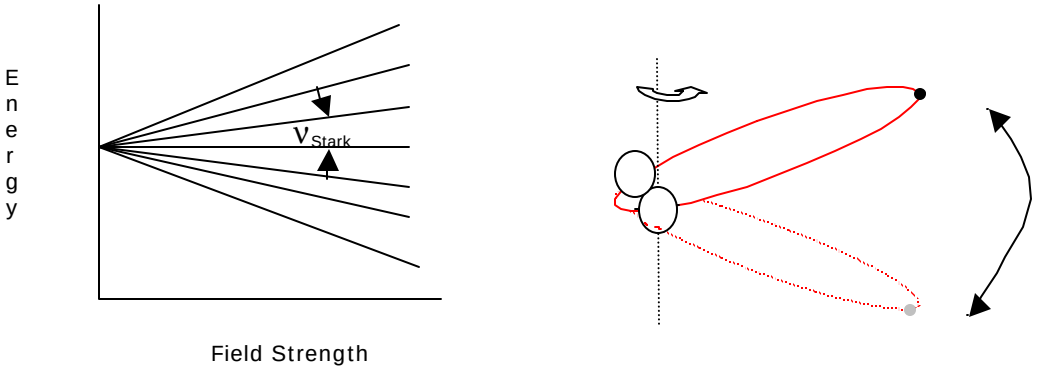

Figure 13: The Stark frequency is equal to the spacing between combs on the manifold(above). Physically it is the rate at which the entire orbit of the Rydberg electron and core precess(below).

$4d_{5/2}(n+2)l'$ states. Above this is another degenerate level at the $4d_{3/2}(n+1)l$ and the $4d_{5/2}(n+4)l'$ levels. This results in a maximum perturbation between the two states. Normally a degenerate state would be pushed upward until Coulomb interactions with the state above stop the rise. In strontium both states are pushed up because of their degeneracies and this results in strong perturbations in this area. The energy relations for this scenario are:

$$E(n)+E_{Stark11}+I_1=E(n+2)+E_{Stark2}+I_2 \quad \textbf{(5)}$$

$$E(n+1)+E_{Stark11}+I_1=E(n+4)+E_{Stark2}+I_2 \quad \textbf{(6)}$$

Subtracting these equations from each other gives:

$$1/n_{3/2}^{*\,3} + k_{3/2\text{Stark}}F = 1/n_{5/2}^{*\,3} + k_{5/2\text{Stark}}F \quad \textbf{(7)}$$

where k is an integer value and $1/(n_{3/2}^*)^3 = \nu_{ryd.1}$, $1/(n_{5/2}^*)^3 = \nu_{ryd.2}$, $k_{3/2\text{Stark}}F = \nu_{\text{Stark}1}$, and $k_{5/2\text{Stark}}F = \nu_{\text{Stark}2}$. The energy relations also tell us:

$$\Delta E_{\text{finestruc.}} = 1/n_{3/2}^{*\,2} - 1/n_{5/2}^{*\,2} = 1/n_{3/2}^{*\,2} - 1/(n+2)_{5/2}^{*\,2} = n_{\text{Stark}} = 280.34\text{cm}^{-1} \quad \textbf{(8)}$$

From the above equations we show that through manipulating the electric field we can set up the interactions so that each time the outer electron passes the core, the core is in the same configuration in a time independent view. If the core were isotropic this would not matter because the outer electron would see no change, but since the strontium has a non-isotropic core there is a great deal of interaction between the outer electron and the core. Each time the outer electron passes it causes the core to switch from a $4d_{3/2}$ configuration to a $4d_{5/2}$ configuration, which in turn causes the outer electron to switch from an nl state to an n'l' state as explained before. Under normal conditions the frequencies of the outer electron and core electron would not be synchronized and so the orbiting electron would see an average over all the states. By adjusting the field we cause the frequencies to be synchronized such that when the outer electron comes close to the core, the core is always in the same orientation. This gives the orbiting electron a kick causing it to switch states and be constantly perturbed.

IV. Experiment

A. Lasers

Three lasers excited the strontium to Rydberg levels, two tunable dye lasers and a commercial tunable dye laser, the Quantaray PDL. A 10Hz Nd:YAG laser pumped all three lasers. A Nd: YAG laser is a Yttrium Aluminum Garnet crystal doped with neodymium (Nd^{3+}) ions. It produces infrared light and then the light passes through two more crystals, each producing another harmonic, one in the visible and one in the ultraviolet. The UV pumped the first and third excitation and

the visible pumped the intermediate laser.

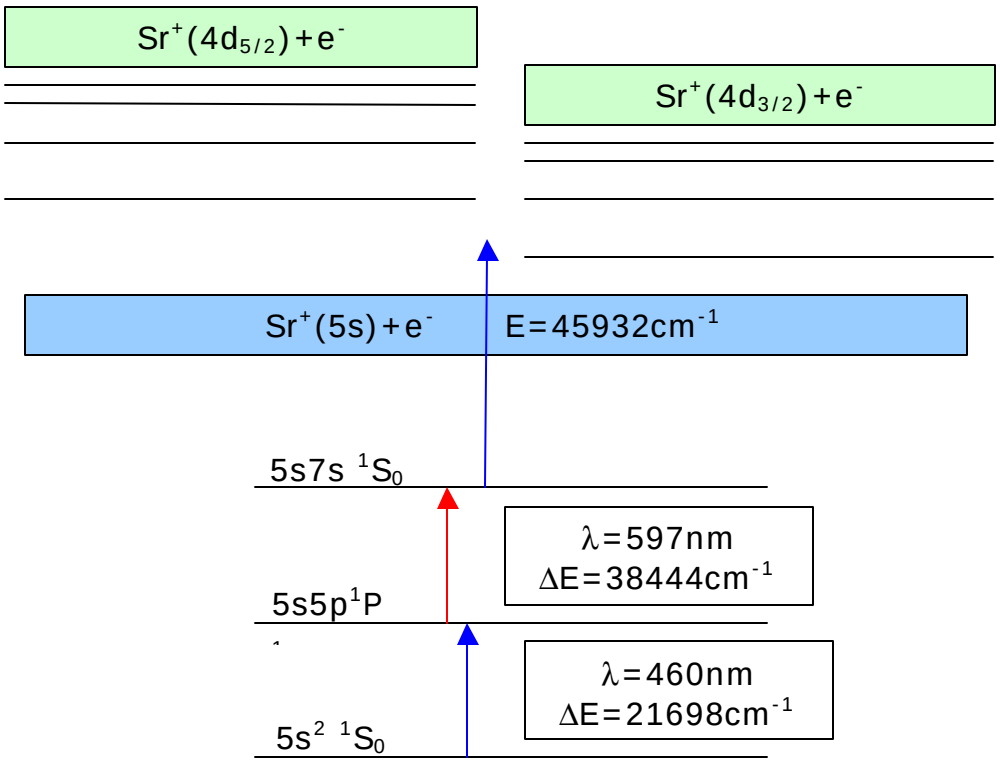

Figure 14: Three-photon step-wise excitation excited strontium to 4dnl levels. The states and energies used are shown above.

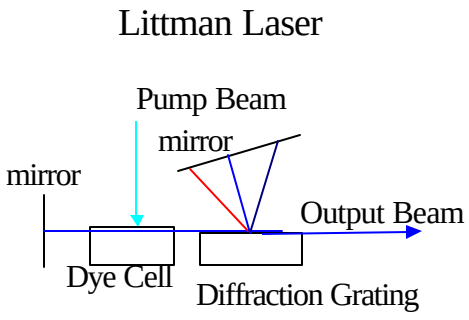

Figure 15: Littman dye laser used to reach first state.

A Littman dye laser with Coumarin 450 brought the strontium from the ground state $5s^2\ ^1S_0$ to the first intermediate state 5s5p $^1P_1$. A Littman dye laser, shown below, uses a diffraction grating to disperse the beam onto a mirror, this allows the wavelength to be tuned over a range. The source beam, the third harmonic of the Nd: YAG (λ = 332 nm), passed through a cylindrical lens

focusing the beam into the dye cell containing, Coumarin dye. The dye absorbed energy from the UV light and emitted blue light in all directions. Some light traveled to the high reflector mirror, back through the cell to the diffraction grating, where the light was bent to the flat mirror then reflected back through the same path. This constitutes the cavity of the laser. The angle the light strikes the mirror off the diffraction grating determines the wavelength of the output light. The only light that will reflect back to the grating from the mirror is light that strikes the mirror normal to the surface. By changing the angle of the mirror the laser can be tuned through a range of wavelengths. We tuned this laser to 460nm to maximize the $5s5p^1P_1$ excitation. This excitation photo-ionized the strontium atoms allowing them to be detected.

From the $5s5p\,^1P_1$ state a Littrow laser excited atoms to the $5s7s\ 1S_0$ state. A Littrow laser uses a prism and a diffraction grating to disperse the beam. Second harmonic light, $\lambda = 532$ nm, from the Nd:YAG focused by a cylindrical lens illuminated the dye cell containing Rhodamine 610. Red light emerged from the dye cell, reflected off of a flat mirror, re-entered the cell and was then dispersed through a diffraction grating by a prism.

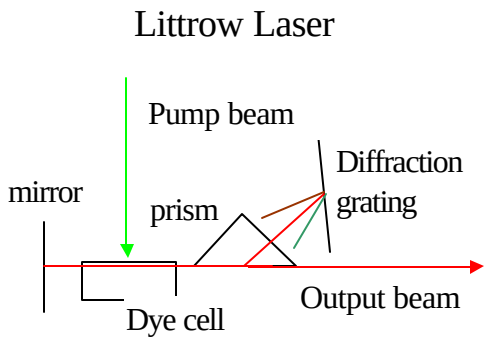

Figure 16: Littman dye laser brought strontium its intermediate level.

The angle the light reflects off the prism into the diffraction grating determines the wavelength of the output light. Only wavelengths striking the grating perpendicular will be reflected back into the prism. The laser is tuned by changing the angle of the diffraction grating. We tuned this laser to 597nm to maximize the $5s7s\,^1S_0$ population. The first and second produced a two-photon signal by entering the chamber at the same time photo-ionizing the strontium making detection possible. Later we delayed the second laser with mirrors to reduce this signal so that we could see the three-photon signal the strongest. Since the three-photon signal was so strong it overpowered the weaker two-photon signal.

The Quantaray lasers excited the atoms past the $Sr^+(5s)$ ionization limit. It is a commercial dye laser containing Coumarin 102 and a cavity with a Littrow dye laser followed by two amplifiers. Using a stepping motor the laser scanned over the 460-467nm wavelength range increasing in increments of 4 motor counts with each step. 1 motor count corresponds to .016nm.

In order to achieve step-wise excitation the three lasers had to arrive at the correct times. The order of the excitation can be seen in figure 17; first the blue laser excited the strontium, then the red laser, and lastly the Quantaray. If the

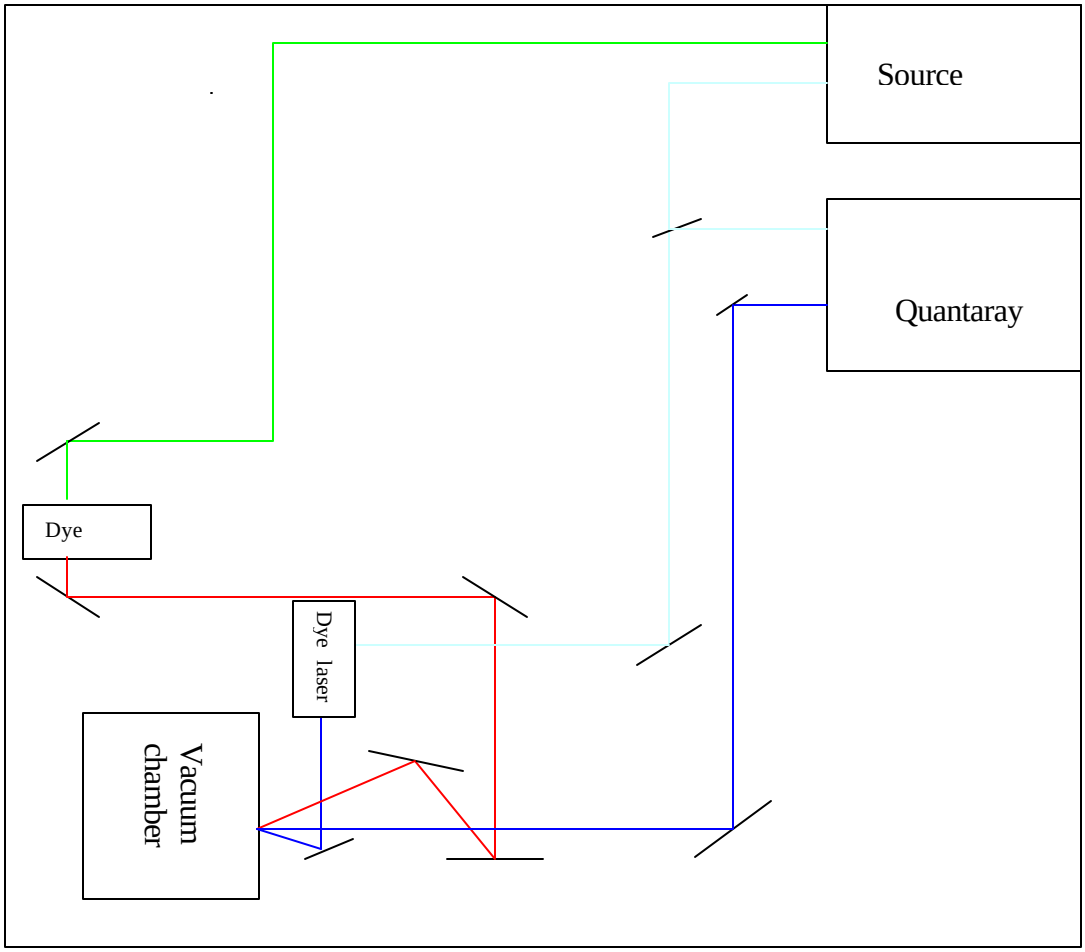

Figure 17: Schematic of table set up. The lasers had to be timed correctly so that the needed transitions could be achieved.

lasers did not arrive in this order then three-photon excitation would not be seen as strongly because the background from the other signal would be much stronger. To prevent this from happening the lasers were distanced from each other on the table. As can be seen below the order of arrival was the blue laser, followed by the red laser and then the Quantaray laser. The red laser was still too close to the apparatus so extra mirrors delayed the beam before it entered the chamber.

B. Apparatus

Three lasers entered the apparatus containing a vacuum chamber, an oven producing the atomic beam, and a detector. A fore pump evacuated the chamber to

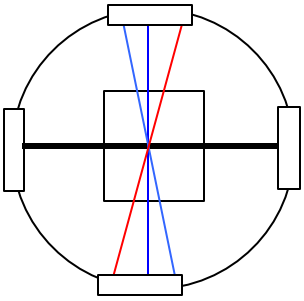

Figure 18: The lasers and atomic beam all overlapped in the center of the apparatus. Alignment of these four beams was imperative to the experiment.

a pressure of about 10^{-2} Torr and then diffusion pump brought the chamber down to 10^{-5} Torr.

The oven was a strontium filled thin wall steel tube with a small hole poked in it. Heating the oven vaporized the strontium producing an effusive atomic beam. Three laser beams entered the chamber perpendicular to the strontium beam as shown in the figure. The four beams were aligned and adjusted until the amplitude of the resulting signal was maximized.

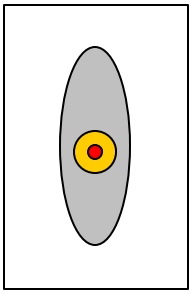

Figure 19: Heat shields guarded the front of the oven. A small hole in the oven forced an atomic beam into the chamber.

The beams propagated between two grounded metal plates. As the strontium auto-ionized, ions and electrons were left between the plates. For the zero field data a pulser sent an electrical pulse in after the three lasers arrived. We detected ions so this positive pulse pushed ions to the detector. The front plate had

a negative high voltage, which attracted the ions. The back plate was grounded causing a potential between the front and back plate. As the ions hit the front plate, electrons were ejected off the plate and pulled towards the grounded plate. Hitting the grounded plate produced more electrons, which traveled to the oscilloscope. For field spectra a constant electric field was applied to the plates. The detection process was identical to the zero field case except instead of a pulse being sent in after the lasers, a constant voltage was applied to the plates.

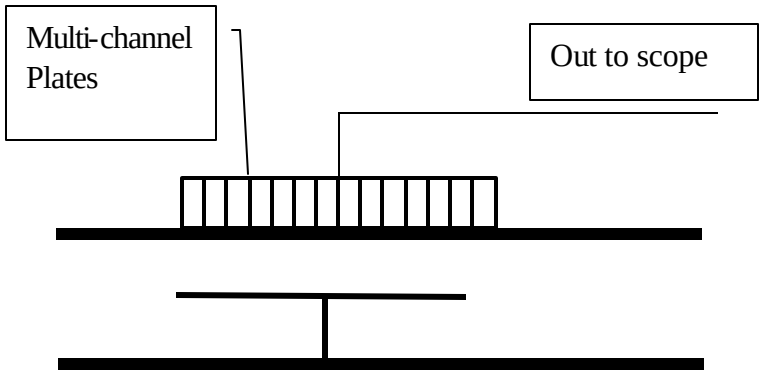

Figure 20: Ions and electrons sat above the metal plate then a voltage was applied that propelled the particles into the detector. The voltage applied to the plates determined which particle was detected.

C. Calibration

When we tune through frequencies with our third laser we must know what frequencies we are tuning through. The first attempt to determine the current frequency was through the counter reading on the stepping motor. The counter reading is a good start but it has its problems, there is an offset that exists as well as imperfections in the drive mechanism. A better calibration mechanism was needed for our experiment. One calibration is an absolute frequency determination, but this is difficult because it only determines one point. We could not use the zero field data for an absolute frequency calibration because the spectrum was not well behaved and broad states make absolute identifications difficult. A second calibration is a relative

frequency determination. An etalon provided a relative frequency determination. A solid glass etalon coated at each surface formed a cavity as shown:

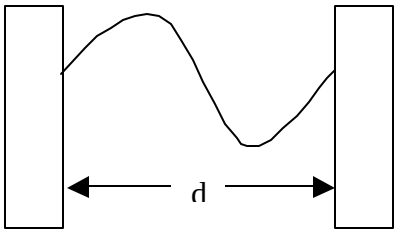

Figure 21: Cavity formed by etalon.

The only waves allowed in this cavity are those with the form of standing waves fixed at both ends governed by the condition:

$$d = N*(\lambda/2) \quad \textbf{(8)}$$

where N is an integer value, λ is the wavelength, and d is the distance between surfaces. This leads to a frequency of:

$$\nu = N*(c/2nd) = N*(\text{FSR}) \quad \textbf{(9)}$$

where c is the speed of light and n is the index of refraction for glass,1.5.

The free spectral range is equal to the distance between frequency peaks of the etalon, as shown below we found a free spectral range of 3.5cm^{-1}. This pattern gives us a set frequency with which we can gauge our spectra. The free spectral

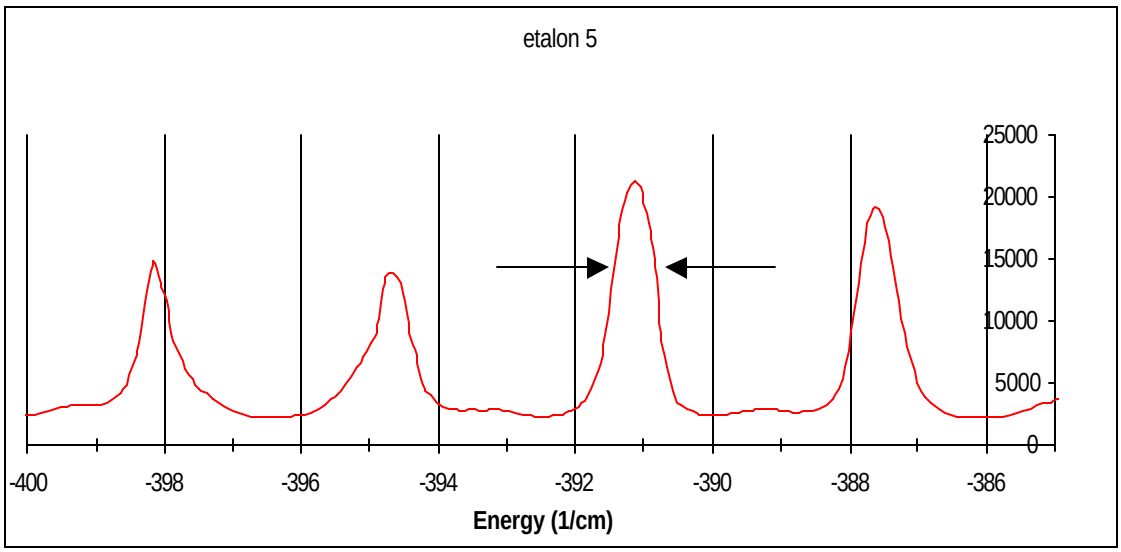

Figure 22: Etalon sweep showing constant frequency distribution.

range is reduced by the finesse of the etalon, the finesse, F, of the etalon which is given by:

$$F = \pi R^{1/2}/(1-R) = 2*(FSR)/FWHM \qquad \textbf{(10)}$$

where R is the reflectivity of the mirrors. The finesse tells the peak sharpness, it is the ratio of the full width at half max (FWHM) to twice the separation of adjacent fringes. Our etalon had a finesse of 20 and an FSR of 3.5cm^{-1}, so:

$$FSR/F = 3.5cm^{-1}/20 = .16cm^{-1} \qquad \textbf{(11)}$$

this ratio tells us that we can measure relative wavelengths to a frequency .16cm^{-1}.

The linewidth of the laser can be deduced from the peaks in the spectrum. The sum of all the broadening agents together can be no worse that the width of the narrowest line. Shown in Fig. 23, the narrowest line in our spectrum taken in a field of 1000V/cm, its width is equal to 0.5cm^{-1}.

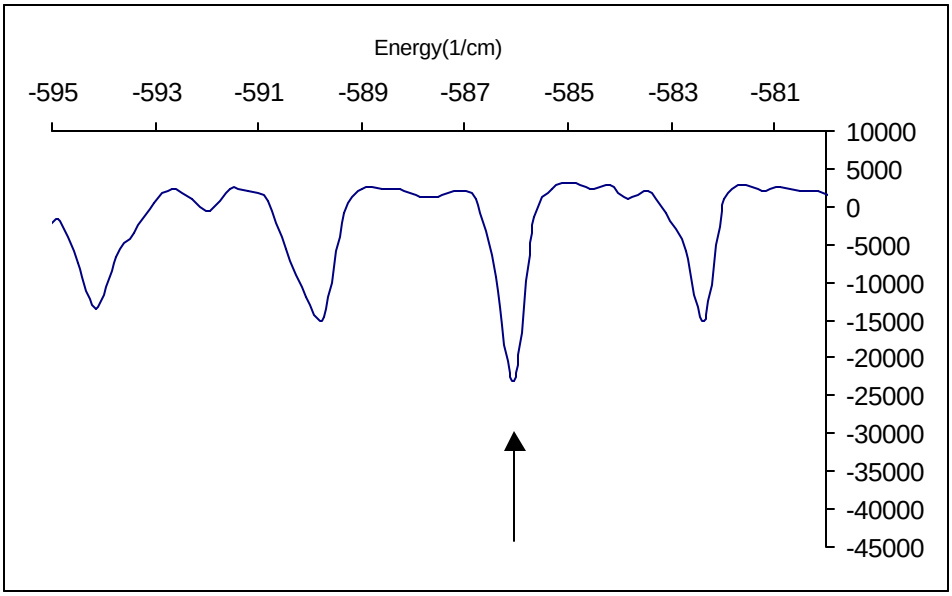

Figure 23: Narrowest peak in our spectra tells a limit on the linewidth of our laser. The sum of all the broadening agents can be no greater than the width of the narrowest line. Shown above it is equal to .5cm^{-1}.

IV. Data Analysis

To understand the energy shifts of the states in an electric field, we first needed to know the capabilities and calibration of our laser system. The zero field spectra allowed us to do this by identifying the states and determining relative frequencies in conjunction with an etalon. Data was collected in the region for $5<n_{3/2}<20$. The basic characteristics of the spectrum are that there are six states converging to two ionization limits: two p-states and an f-state converging to the lower ionization limit and one p-state and two f-states going to the higher ionization limit. This zero field data convinced us of the complexity in strontium's structure:

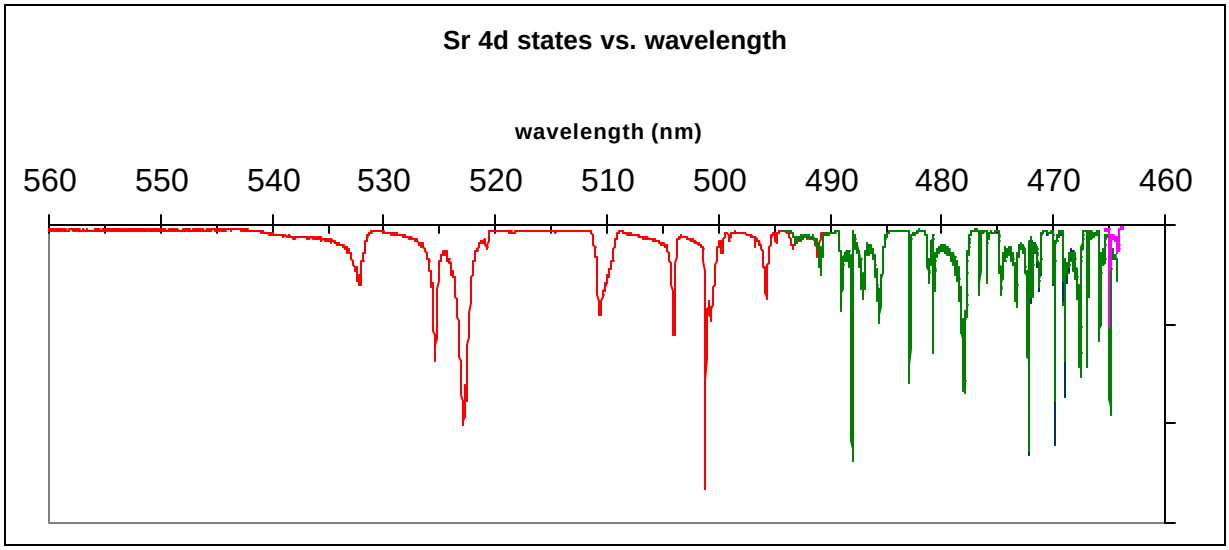

Figure 24: Zero field spectrum of strontium plotted versus wavelength (nm).

This data shows the problems that occurred in the zero field spectra. Auto-ionization makes states broad and strong perturbations make the states indistinguishable. It is unclear from the data which states are converging to which series. Plotted versus $n^*_{3/2}$ or $n^*_{5/2}$ one should be able to see the pattern of three states converging to the $4d_{3/2}$ series and three converging to the $4d_{5/2}$ series. Clearly this is not the case:

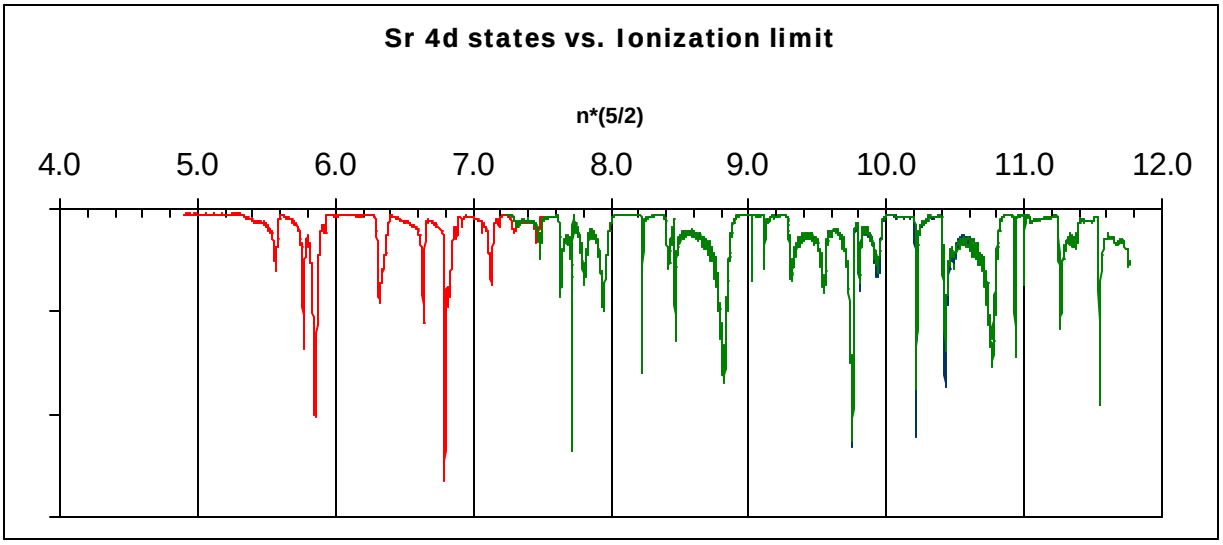

Figure25: Strontium plotted versus $n_{5/2}^*$, three lines in the spectrum should converge on this series, clearly they do not.

We identified low-lying states by comparing our spectra to the VUV spectra of Hudson (et al.). As can be seen in Fig. 26 the correlation was good:

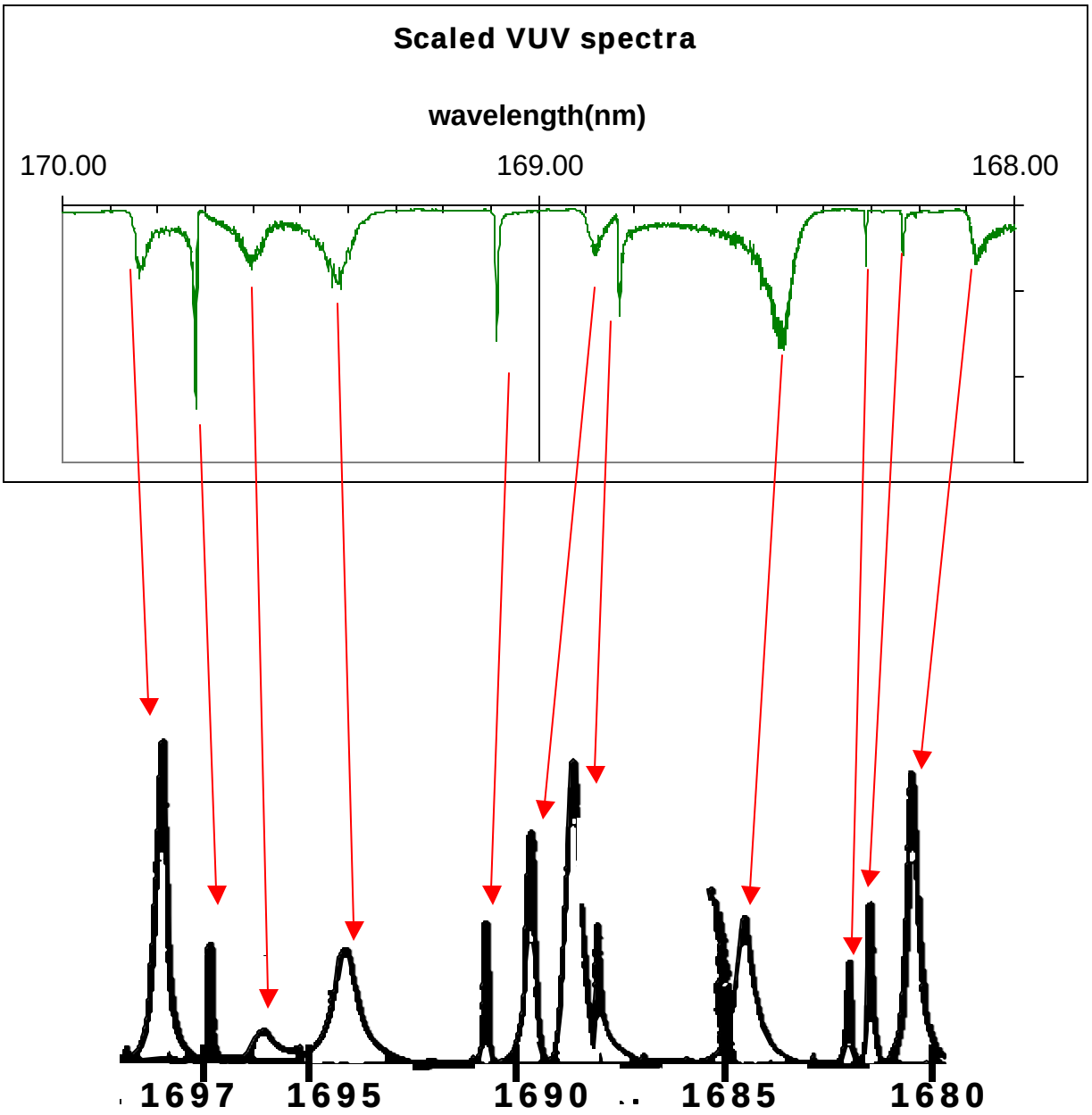

Figure 26: Scaled spectra to compare the VUV spectra taken by others. As can be seen our data(above) correlates well with Hudson's data taken in 1969(below).

The relative peak positions are the same. This did not give us ultimate identifications though because the states are so mixed it is difficult to say which is a p state and which is an f state. Instead most of the peaks are a superposition of the two or more states.

Beyond the perturbed region we thought the spectrum may be more straightforward and a pattern would be evident. We looked at higher n values to see if this was the case, it was not:

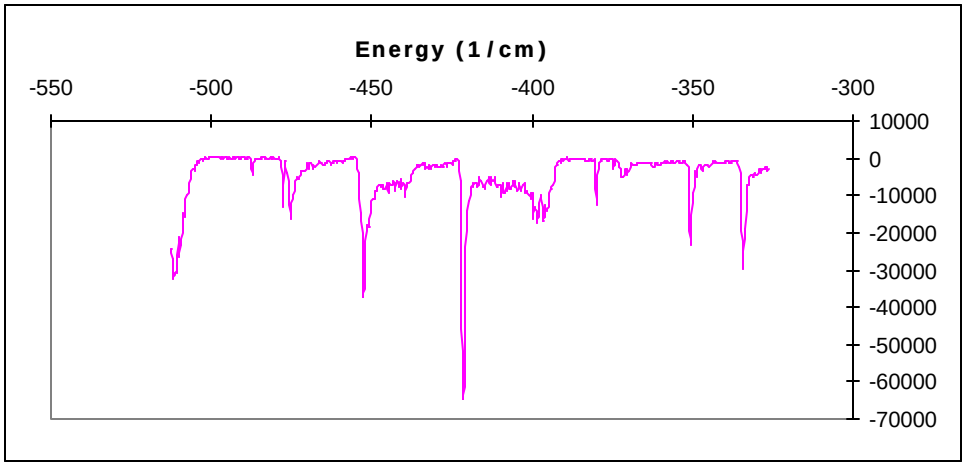

Figure 27: Data at higher n values, again there is no observable pattern.

In zero field strontium is extremely difficult to understand. Due to the broad states, configuration mixing, and degeneracies the spectrum is nearly impossible to characterize. What is known about the spectrum in zero field is that there are six states converging to two ionization limits. The states are strongly perturbed and no consistent pattern is evident.

A. Electric Field

The problems in zero field were broad states due to auto-ionization and strong perturbation resulting in configuration mixing. Applying an electric field solved both of these problems. A field destroys the symmetry of the core allowing high l states to couple to low l states with the same magnetic quantum number m. High l states have no density in the 4d core so they do not orbit the core as closely as in the zero field case. In response the core loses its n dependence in its wavefunction and relaxes. Therefore the orbit radius of the outer electron increases so the outer electron does not orbit as close to the core. The complex interactions between the core and orbiting electron are reduced, making the spectrum clearer. The other big problem was broadening due to auto-ionization. In a field auto-ionization is reduced. The $1/r_{12}$ interaction weights the closest approach, this distance is approximately equal to l. Since the high l states do not penetrate the core this distance, r_{12}, is increased and the $1/r_{12}$ interaction becomes weak. The auto-ionization rate depends on $\left|<(1/r_{12})>\right|^2$, so as the distance increases the rate is reduced. The auto-ionization rate is averaged over all of the states involved, so in a field when many states couple together, the auto-ionization rate is spread out over them.

This results in more narrow states and makes identification easier. The above is clearly seen in the preliminary spectrum in Fig. 28, taken in a field of 1000V/cm:

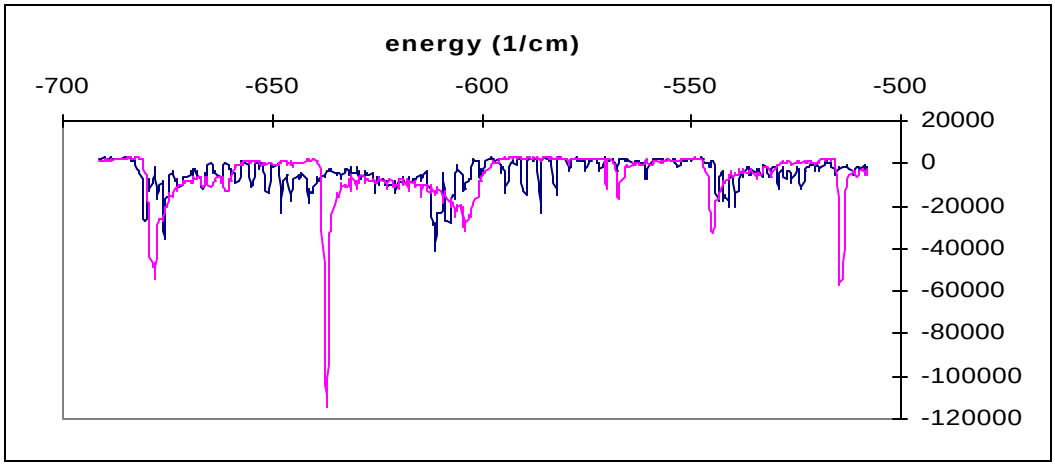

Figure 28: Spectra in a field (blue) compared to the same spectra in zero field (pink). Clearly there is Stark splitting.

Later data shows that Stark structure is present and mostly follows the hydrogenic model except in the areas where the series overlap. In this area of perturbation spectral lines anti-cross and the spectrum is more complicated as

expected. As illustrated in Fig. 29 we expect to see areas of hydrogenic Stark splitting and areas of non-hydrogenic Stark splitting:

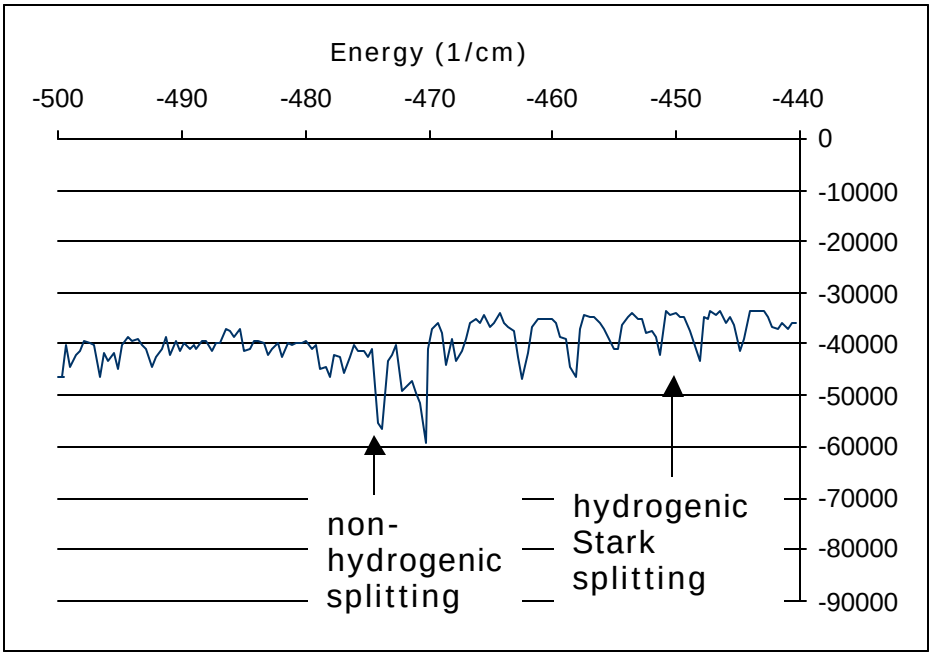

Figure 29: Data taken in a higher field. Stark splitting is clearly evident, regions of both hydrogenic and non-hydrogenic splitting.

B. Laser Resolution

There are three things that limit the resolution of our lasers: auto-ionization, laser linewidth, and electric field inhomogeneities. We determine the precision of our lasers by looking at the spectra and finding the narrowest feature, our lasers are at least as precise as the width of the narrowest peak. As shown before our most narrow peak was .5cm^{-1}. This gives us a boundary on the capabilities of our lasers. Our precision can be no worse than .5cm^{-1} because the sum of all the broadening agents combined can produce lines not more narrow than .5cm^{-1}.

The peak widths in our spectrum give us a bound on the auto-ionization rate. In zero field the broadest peak was 12.5cm^{-1}. In a field the widest peak was 2.27cm^{-1}. Therefore the auto-ionization rate is reduced by a factor of 5.5 in a field.

Our field data tells us about the field inhomogenieties in our electric field. By looking at the shift that occurs on the edge of one of the stark manifolds and dividing

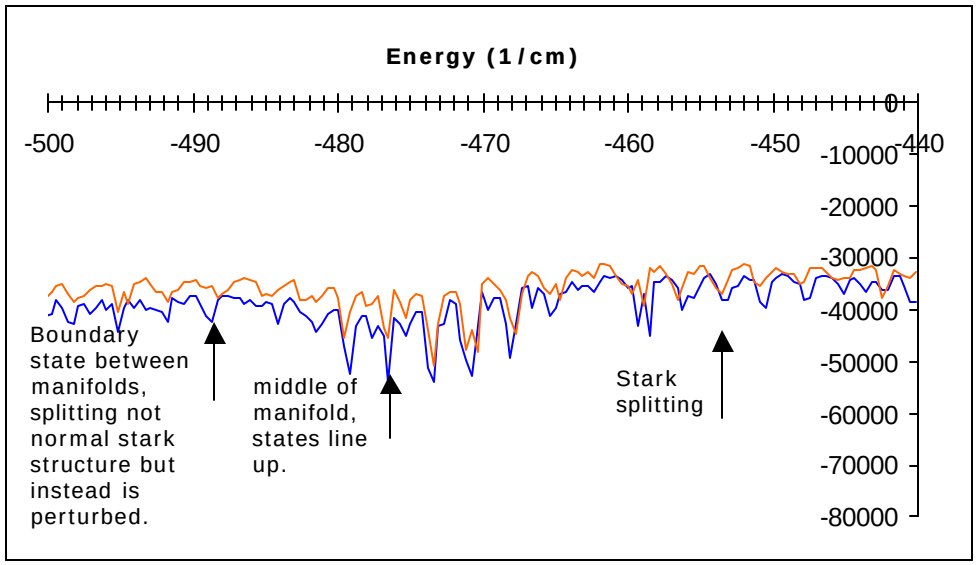

Figure 30 : Spectra in a field. The states in the middle of the manifold remain unperturbed, on either side the states are shifted, in some areas the shift is not the normal pattern that one would expect because the states are strongly perturbed in these areas.

by half the width of the manifold, the field inhomogeniety can be found. Figure 30 shows a spectra taken in a field of 1066V/cm and the same spectra in 1000V/cm. Even with a field difference of 66V/cm the shifts can be seen. The field inhomogeniety can be determined by looking at a state of the edge of the manifold and calculating the ratio between its width and its distance from the middle of the manifold. Shown in figure 31, a state on the edge of the manifold has a width of .4cm^{-1} and its distance from the center of the manifold is 30cm^{-1}, so:

$$.4\text{cm}^{-1}/30\text{cm}^{-1}=.013 \qquad \textbf{(12)}$$

Therefore we know our field inhomogenieties to 1.3%.

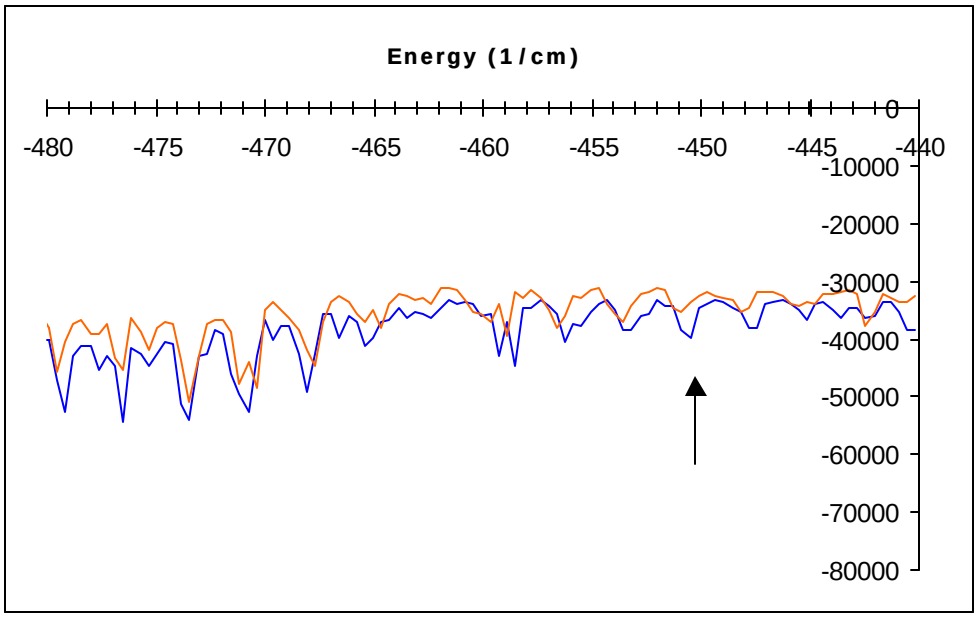

Figure 31 : The state above is on the edge of the Stark manifold. Its width is .4cm^{-1}, when compared to its distance from the center of the manifold the field inhomogeniety can be calculated.

V. Conclusions

We have shown that precision measurements of strontium in an electric field are possible. In zero field the spectrum is complicated due to broadening from auto-ionization and configuration mixing of perturbed states. Applying a field greatly simplified the situation and made state identification possible. Limiting factors of the spectroscopy were laser precision, field inhomogenieties, and broadening from auto-ionization. We showed the limits on these parameters achievable with our system. Future data awaits information from the theory group about electric field strengths and the precision needed to measure shifts in the spectra.

VI. Future Work

Future work in this area includes a closer study of the field data as well as scaled spectroscopy. This is a technique where the electric field strength and energies being scanned over are simultaneously changed. This would allow periodic orbits to be seen if they exist. Another possibility is to see if similar problems occur in other alkaline earth elements to determine whether the problem is unique due to the structure of strontium or if it exists elsewhere.

VII. Acknowledgements

I would like to thank Dr. Cooke for his help, patience, guidance, and support both this year and the previous years I have worked with him. He is an inspiration to his students. I would also like to thank Ken Baranowski for four years of friendship and the countless hours spent in lab working out all the problems that arose.

VIII. References:

[1] R. Hudson, V. Carter, P. Young, Phys. Rev. **180**, 77 (1969).
[2] P. Esherick, Phys. Rev. A, **15**, 2920 (1997).
[3] M. Aymar, E. Luc-Koenig, S. Watanabe, J. Phys. B: At. Mol. Phys. **20**, 4325 (1987).
[4] M. Aymar, J. Phys. B: At. Mol. Phys. **20**, 6507 (1987).
[5] M. Kompitsas, S. Cohen, C. A. Nicolaides, O. Robaux, M. Aymar, P. Camus, J. Phys. B: At. Mol. Phys. **23**, 2247 (1990).
[6] M. Kompitsas, S. Goutis, M. Aymar, P. Camus, J. Phys. B: At. Mol. Phys. **24**, 1557 (1991).
[7] C. Greene, M. Aymar, Phys. Rev. A **44**, 1773 (1991).
[8] J. Neukammer, H. Rinneberg, J. Phys. B: At. Mol. Phys. **15**, 3787 (1982).
[9] D. Harmin, Phys. Rev. A, **24**, 2491 (1981).
[10] K. Sakimoto, J. Phys. B: At. Mol. Phys. **22**, 2727 (1989).
[11] K. Sakimoto, J. Phys. B: At. Mol. Phys. **19**, 3011 (1994).
[12] H. H. Fielding, T. P. Softley, Phys. Rev. A **49**, 969 (1994).
[13] H. H. Fielding, T. P. Softley, Chem. Phys. Lett. **185**, 199 (1991).
[14] J. Neukammer, H. Rinneberg, J. Phys. B: At. Mol. Phys, **15**, 3787 (1982).
[15] F. Robicheaus, C. Wesdorp, L.D. Noordam, Phys. Rev. A, **60,** 1420 (1999).